Communications with Guaranteed Low Latency and Bandwidth using Frequency Referenced Multiplexing

Zichuan Zhou
University College London
Jinlong Wei
Huawei Technologies Duesseldorf GmbH
Yuan Luo
the Chinese University of Hong Kong (Shenzhen) https://orcid.org/0000-0001-5129-0130
Kari Clark
University College London https://orcid.org/0000-0003-1988-3205
Eric Sillekens
University College London
Callum Deakin
University College London
Ronit Sohanpal
University College London
Radan Slavík
University of Southampton
Zhixin Liu (zhixin.liu@ucl.ac.uk)
University College London https://orcid.org/0000-0002-9681-7933

Article

Keywords:

Posted Date: April 26th, 2022

DOI: https://doi.org/10.21203/rs.3.rs-1558939/v1

Communications with Guaranteed Low Latency and Bandwidth using Frequency Referenced Multiplexing

Zichuan Zhou[1], Jinlong Wei[2] ✉, Yuan Luo[3] ✉, Kari A. Clark [1], Eric Sillekens[1], Callum Deakin[1], Ronit Sohanpal[1], Radan Slavík[4], and Zhixin Liu[1] ✉

[1]Optical Networks Group, University College London, London, UK
[2]Huawei Technologies Duesseldorf GmbH, European Research Centre, Munich, Germany
[3]The Chinese University of Hong Kong (Shenzhen), Shenzhen, China
[4]Optoelectronic Research Centre, University of Southampton, Southampton, UK
[1]zhixin.liu@ucl.ac.uk
[2]jinlongwei2@huawei.com
[3]luoyuan@cuhk.edu.cn

Abstract

The rise of timing-critical applications such as virtual reality and connected car fleets, combined with the rapid growth of the number of user devices, creates new challenges for the latency and reliability of user-cloud data communications. Currently user-cloud communications rely on time-scheduled data frames through tree-topology fibre networks, incapable of assuring guaranteed connections with low or stable latency, which is necessary for, e.g. remote surgeries and safe operations of self-driven cars. Besides, their scalability to a larger user count is limited. Here we show that clock and optical frequency synchronisation, enabled by burgeoning frequency comb and signal processing techniques, can provide each user with dedicated optical bandwidth to enable scalable user-cloud communications that guarantees simultaneously high per-use data rate and low latency. Our approach provides accurate clock and optical frequency synchronisation over deployed optical fibre links, which will be beneficial for many applications including accurate navigation, quantum communications, and astronomy.

1 Introduction

Two decades of vigorous growth of cloud services have made them an indispensable part of our everyday lives. It is expected that emerging applications such as virtual reality (VR), augmented reality (AR) and intelligent autonomous vehicles will continue to drive the exponential growth of global data traffic into the next decade [1]. These trends have been captured by several analyses indicating that the optical broadband traffic will octuple or even decuple in a decade [2, 3] and therefore the user bandwidth must scale accordingly to keep up with the demand [4]. These predictions have motivated the active development of electronic and opto-electronic components to 100 GHz bandwidths and beyond [5, 6, 7, 8, 9, 10, 11, 12]. These estimates contribute to the conventional wisdom [13, 14] that as demand for broadband traffic rises rapidly, so too must the end-user bandwidth. Nevertheless, though these extrapolations based on traffic growth are true for long-haul and point-to-point systems, this conventional wisdom will not apply to future user-cloud access networks due to the strong countervailing trends of the growth in the number of user devices (e.g. virtual reality headsets, traffic sensors) and their demand for guaranteed connections as well as low and stable latency to edge data centres [15, 16, 17, 18].

Here, we integrate recently-published data for VR/AR and intelligent vehicles (see figure 1), showing a radical growth in their numbers within the next decade. This data, together with the stringent requirement of low and stable latency [19], which will need to be guaranteed to, e.g. ensure traffic safety, rather than provide at the 'best effort' bases as today, when an average or mean latency is often used as a metric [18, 20]. All these aspects represent the following new technical requirements of future user-cloud communication infrastructures:

- They should provide low and stable latency connection in conjunction with the ability to scale across a large number of users, each with a few Gbit/s-level data rate [21, 22, 23] (data summarised in details in Table 1).
- They should provide a highly accurate synchronised clock to enable sub-nanosecond time synchronisation. For example, VR and self-driving car fleets require low-cost and highly scalable time synchronisation infrastructure to enable sub-meter scale positioning of devices [24]. Although sub-nanosecond time synchronisation is achievable using GPS, it is costly and relies on line-of-sight to the sky, which is difficult or impossible underground, within buildings or in urban canyons [25], and may be inhibited by atmospheric ash during volcanic eruptions or wartime [26]. Therefore, sub-nanosecond time synchronisation through the already deployed optical fibre access networks is highly desired.
- They should enable reconfigurability for various on-demand services with flexible modulation formats or bandwidths to support widely varying applications [23, 27]. For example, co-operative concerts through the internet only require a moderate data rate but have a stringent requirement of low and stable latency. Low order formats such as quadrature phase shift keying (QPSK) should be used to provide low bit error rate (BER) and forward error correction (FEC) free signalling to minimize latency and power consumption [16]. Remote education and remote work, however, require a high data rate to transmit high resolution video with a relaxed tolerance to latency. Thus, high order formats such as 16 quadrature amplitude modulation (QAM) could be used [28].
- They should also be compatible with legacy infrastructures such as existing mobile fronthaul and passive optical networks for low-cost deployment [29].

Current user-cloud data transmission relies on time division multiplexing (TDM) approaches through passive optical networks (for households and buildings) [30, 31] or radio access networks (to base stations and radio units) [32] to provide user-cloud data communications, with both employing tree-topology passive-split fibre links for cost-efficient deployment. Although the cloud-to-user data transmission, known as downstream, can be easily achieved using broadcasting and media access control (MAC) layer protocols [33], the user-to-cloud (upstream) transmission presents a major challenge due to the random and bursty nature of data generated from the users. To avoid contention when multiple users send data simultaneously, time scheduling and buffering of data frames with a large gap in between is required for user registration and dynamic bandwidth allocation (minimum 250 µs due to protocols involving several two-way handshakes [34]), leading to an unavoidably large and unpredictable latency [17]. This not only negatively impacts user experience, but also presents potential high risks for user safety in applications such as remote surgery and autonomous vehicles, leading to a recent debate for legislation to provide guaranteed connection for autonomous car fleets [20].

An alternative to the currently-used TDM approach is wavelength division multiplexing (WDM) [35, 36] , which offers dedicated bandwidth to each user and therefore promises guaranteed, low and stable latency user-to-cloud communications. The drawbacks that have prevented this technology from being implemented more widely is the high cost, as it requires WDM components for every remote node and user. Combined WDM-TDM approaches [37] support more users with a lower cost than a WDM-only solution, but the use of TDM still leads to contention and queuing that precludes low and stable latency [38]. Recently, electronic sub-carrier multiplexing (SCM) techniques using coherent transceivers have emerged to overcome these challenges and provide software-defined, bandwidth-flexible cloud-user connections [29, 39] . However, this requires expensive broadband (>50GHz [29]) digital optical coherent transceivers with power-hungry application-specific integrated circuits (ASICs) for every user. This high power consumption and cost runs counter to the need for low cost and low power digital infrastructure [40].

Finally, current access networks cannot provide scalable and low-cost time synchronisation with sub-nanosecond accuracy. The low-cost time synchronisation protocols, such as the precision time protocol (PTP), only achieve microsecond accuracies due to clock frequency deviation between device clocks [41]. A possible solution would be to implement rubidium atomic clocks, but equipping each user with such high-cost and high-power-consumption device would be impractical. A more viable solution is therefore user device clock synchronization at ns-level. However, current approaches such as Synchronous Ethernet [42] have up to 20ns time error and are not highly scalable [43]. A highly-scalable and low cost technique to clock synchronise end-user devices with sub-nanosecond accuracy is currently lacking.

Here, we overcome all the aforementioned challenges using a closely-spaced frequency division multiplexing (FDM) method to provide dedicated bandwidth for every user, enabling contention-free, clock-synchronised user-cloud upstream communication. Although this represents an WDM-only approach, it

does not require expensive WDM components at the remote node and user side, addressing the main drawback of WDM, i.e. the cost. We achieved this by disseminating a frequency comb to all users, which permits clock synchronisation and optical carrier frequency synchronisation using low-speed frequency locking, facilitating upstream FDM transmission over existing colourless passive power splitting fibre networks. It does not require any modification of deployed fibre infrastructure (i.e. our FDM approach uses conventional deployed TDM networks) and is made practical by the maturation of technologies including frequency comb generation [44, 45], low-cost narrow linewidth lasers [46, 47], laser frequency control [48, 49] and digital optical coherent receiver techniques [50].

This approach grants all users dedicated optical bandwidth for upstream data transmission without the need for time scheduling or data buffering, ensuring highly-reliable constant user-connections with low and stable latency. Our optical clock dissemination approach permits synchronised clocks for all users, providing low-jitter, highly-scalable clock synchronisation essential for sub-nanosecond timing synchronisation using PTP or SynchE [41, 42]. Further, the user transceivers only require low speed electronic and opto-electronic components (1.25 GHz in our demonstration) to transmit signals at baseband. This significantly saves the cost and power consumption of the transceivers compared to the current TDM approach, which requires each user to operate a full rate. For example, in 50 Gb/s TDM system [34, 51], each user requires a 25 GBd transceiver whilst the average per-user data rate is less than 800 Mb/s (assuming 64 users).

In this article, we demonstrate frequency comb generation with more than five hundred 2.5-GHz-spaced tones with less than 10 dB power variation, providing clock synchronisation to user transceivers with a <4 ps root-mean-square (rms) timing jitter (integrated over 1 kHz to 10 MHz) and a <10-kHz linewidth optical carrier. Using a low-cost frequency stabilisation method, we demonstrate FDM of 64 user signals with different modulation formats, promising up to 320 users with all five demonstrated WDM bands. Up to 4.3 Gb/s per-user data rate and a total capacity of 240 Gb/s is achieved in a single 200-GHz WDM band, providing sufficient per-user data rate for time-critical applications. The radical new approach presented here promises a viable route to a scalable, future-proof, low-power and low-latency user-cloud access technology for future time-critical applications.

2 Results

2.1 Clock and frequency referenced system architecture

At the core of our system is an optical frequency comb placed at the edge cloud, which is distributed to users/customers to provide them with both a clock and optical carrier frequency reference (figure 2a). The optical frequency comb is seeded by a narrow linewidth laser to produce a low noise optical frequency reference and the tone spacing is locked to a reference clock to enable clock distribution. The large number of optical frequency comb tones enables FDM for a large number of users (e.g. up to 320 users in this demonstration). The comb tones within the same WDM channel (e.g. 100-200 GHz bandwidth stated in the ITU-T standard) are routed to users in the same region (figure 2e), who are connected to the same passively split remote node. Each user uses a low-speed photodiode to detect the 2.5-GHz beat note that provides signal for their clock, which is detailed in the following section. Further, the users lock their transmitters to the assigned comb tones (one comb tone per user) and transmit their upstream signals within the designated optical bandwidth. This permits each user to have a dedicated optical bandwidth and synchronised clock for upstream transmission. Figure 2b shows the downstream comb after WDM demultiplexing and routing of each WDM channel to a group of users and figure 2c represents the aggregated upstream FDM signals from users using the same WDM channel.

The aggregated signals are detected and demodulated by a single broadband (160 GHz) optical coherent receiver at the edge data centre. Since the users signals are transmitted and detected within the designated optical bandwidth, the modulation formats and signal bandwidth can be flexibly adjusted to suit different traffic types without affecting other users. In our demonstration, we use low speed (4.9 GSa/s) and high-resolution (10 bit effective number of bits) digital-to-analog converters (DACs) to generate sub-carrier modulation (SCM) signals of different modulation formats. The electroabsorption modulators (EAMs) used have more than 5 GHz opto-electronic bandwidth, permitting adjustable bandwidth to suit different users' demand. Two example user cases are shown in figure 2e.

2.2 Comb generator and clock phase noise

Our optical frequency comb generator and the experimental setup for clock and carrier distribution are shown in figure 3a. The optical frequency comb generator comprises a 10-kHz linewidth seed laser followed by two comb generation stages. The first stage consists of an intensity modulator (IM) and two phase modulators (PM) connected in tandem, all driven with in-phase 25-GHz RF signals to yield a 1.25-THz bandwidth frequency comb with 5 dB spectral flatness (see figure 3b). The second comb generator stage uses two cascaded IM and PMs, both driven with 2.5 GHz RF signals to convert each of the 25-GHz spaced comb tones into a 2.5-GHz-spacing frequency comb with a spectral flatness of 6 dB. By locking the 25 GHz electronic phase lock loop 1 (PLL_1) with the 2.5 GHz PLL_2 to the same 10-MHz clock source, the 2.5-GHz comb signals generated from each 25-GHz-spacing tones are frequency and phase locked, yielding a 1.25 THz bandwidth, 2.5-GHz-spacing comb signals with a spectral flatness better than 10 dB (figure 3c). The comb tones are subsequently amplified to 18 dBm using an erbium-doped fibre amplifier (EDFA) before being WDM de-multiplexed into five 200-GHz WDM grid wavelength channels, each outputting 5 dBm optical power and containing approximately 70 tones (figure 3d). The WDM demultiplexed comb tones are launched into 22 km of standard single mode fiber (SSMF), which emulates the feeder fibre in the optical access links.

The distributed clock is recovered by each user by detecting the comb beat using a 3 GHz bandwidth photodiode followed by 40 dB RF amplification. The detected 2.5 GHz clock signal shows a clean spectrum (figure 3e) and is subsequently divided to 50 MHz (inset in figure 3e) to serve as the reference clock for the user transceivers. We characterised the power budget for the distributed clock by attenuating the de-multiplexed comb signals using a variable optical attenuator (VOA) and calculating the rms timing jitter by integrating the measured phase noise from 1 kHz to 10 MHz. Using channel 4 (shown in orange in figure 3d, 193.4-193.6 THz) as an example, the rms jitter remained below 4ps with the optical power between -3 dBm and -18 dBm. The abrupt increase of jitter when power drops to -17 dBm was due to the failure of the frequency locking of the divider. The increased jitter with high optical power is due to the saturation of the RF amplifiers. These results indicate more than 23 dB power budget available for clock dissemination, permitting a remote node split ratio of more than 64. Subsequently, we measured the phase noise and the integrated jitter of the distributed clock for all WDM channels at a received optical power of -13 dBm. As shown in figure 3g, all WDM channels show sub-2-ps timing jitter, promising similar system performance over the whole wavelength region.

2.3 FDM data aggregation

To demonstrate the clock-synchronised FDM transmission, we carried out a series of experiments using a proof-of-concept system shown in figure 4a. Our system contains three live user transceivers whose lasers are frequency-locked to three neighbouring comb tones, resulting in three 2.5-GHz-spaced FDM signals after being combined by a coupler at the remote node (see figure 4b for spectrum). The user transceivers are synchronised to the optically distributed clock, eliminating any need for clock recovery at the receiver side. We use the same type of single-wavelength lasers (about 150 kHz linewidth [46]) for all transceivers. The continuous wave (CW) signals from the lasers are split by a 50:50 coupler for frequency locking and upstream data transmission. To demonstrate the simultaneous detection of all FDM signals within the same wavelength channel, we generate dummy signals by modulating tapped comb signals after 80-km decorrelation fibre and notch-filtering, shown in green in figure 4c. The aggregated upstream signals transmit back to the edge cloud side and are detected by a pre-amplified coherent receiver with 160-GHz optical bandwidth, centred at 193.407 THz (1550.08 nm). The coherent receiver uses the seed laser wavelength filtered from the 1st stage output as the local oscillator (LO). This not only provides the coherent receiver with a narrow linewidth LO, but also promises a deterministic frequency offset for user upstream signals, eliminating the carrier frequency offset (CFO) estimation in the receiver digital signal processing (DSP). We subsequently measure the bit-error-ratio (BER) performance of the upstream SCM quadrature amplitude modulation (QAM) signals. Different orders of QAM signals (4/8/16 QAM) with a root-raise-cosine pulse shape (roll-of-factor of 0.01) are generated using the user transceivers' digital-to-analog converters (DACs).

To demonstrate ability of each user to lock to any comb tone within the WDM channel necessary for flexible FDM channel allocation, we tune the live users across 160-GHz frequency region (see methods for details), with them always lock to neighbouring comb tones and are combined with dummy signals to populate the 160 GHz bandwidth. Figure 4d shows the measured receiver sensitivities using live user 1 as an example. At the soft-decision forward error code (SD-FEC) bit error rate (BER) threshold of 2e-2 (15.3% overhead [52]), the required lowest power values are approximately -47, -40 and -35 dBm,

respectively, for 4/8/16 QAM formats.

Since the user transceivers output about -4 dBm, these results indicate a power budget of 43, 36 and 31 dB for an upstream per-use data rate of 2.14, 3.22 and 4.3 Gbit/s using 4/8/16 QAM signals, respectively. The relatively low output power was due to the high coupling loss of the used electroabsorption modulator (EAM) in this experiment (about 10 dB). A potential 4-6 dB improvement of power budget can be expected by using low-loss modulators such as the integrated EAM [53]or Mach-Zender modulator (MZM) [6, 7].

Considering a fully populated wavelength channel, the estimated aggregated data rates are about 133, 190 and 240 Gb/s, using 4/8/16 QAM formats, respectively. The reduced power sensitivities at the edge of the optical bandwidth are primarily due to the frequency roll-off of the balanced photodiodes in the coherent receiver. Further, we study the frequency stability of the upstream user lasers. The minimum required power per tone for the frequency lock loop (FLL) is -44 dBm. At -35 dBm power, the maximum frequency deviation is less than 1.5 MHz over 24 hours (figure 4f). The stable frequency indicates that the system only requires a small guard band between neighbouring channels for high spectral efficiency.

3 Discussion

We analysed the data from recently emerging sources and showed that the challenges for future digital infrastructure is how to provide guaranteed connection with low and stable latency for time-critical applications. Our technological novelties to address these challenges include: 1) generation of a 2.5-GHz-space frequency comb using a two-stage configuration which yields a low noise, flat frequency comb with more than 500 tones to act as clock and optical frequency references; 2) dissemination of the frequency comb to users through passive fibre networks, by which we achieved clock and optical frequency synchronization for all users, allowing for dedicated bandwidth for each user using low-cost and low power consumption electronics; 3) demonstration of a proof-of-concept FDM system servicing up to 64 users with an aggregate bandwidth of 160 GHz, showing up to 4.3 Gb/s per user data rate (240Gb/s per WDM channel) with a high receiver sensitivity of -35 dBm.

Although our demonstration uses 200-GHz wavelength demultiplexers for each WDM channel, smaller WDM channel bandwidth (e.g. 100-160 GHz) could be used to fully utilize the available optical spectrum without any gap between neighboring WDM channels. This would straightforwardly increase the number of users to 500 by using multiple coherent receivers to detect signals from all the WDM channels. The number of users could be further increased to more than 1000 by using more wavelength channels within the low loss telecom C band, e.g. 1540-1562nm. Wide-bandwidth flat spectra combs have been demonstrated in this wavelength region using cascaded opto-electro modulators [44], optical parametric mixing [45] or a combination of both techniques [54]. Although the demonstrated frequency combs have >25 GHz tone spacing, they can be easily engineered to smaller spacing using a second stage as we have demonstrated. Importantly, erbium-doped fibre amplifiers (EDFAs) with high and flat gain over 1535-1565 nm wavelength region are readily available to ensure sufficient power budget for the clock and optical frequency synchronisation.

In addition to providing guaranteed bandwidth, our approach also significantly reduces the RF bandwidth of user transceivers by a factor of N (where N is the number of users connect to the same remote node) compared to the conventional TDM approach. This allows for a significant reduction in power consumption and packaging costs as well as enhanced jitter tolerance and fundamentally higher receiver sensitivities due to the reduced baud rate. The reduced user transceiver bandwidth also permits using high resolution DAC that cannot be achieved in high baud rate signaling [55], enabling high-performance constellations or probabilistic-shaping DSP to improve dynamic range and receiver sensitivity [56]. Besides offering flexible modulation formats, the bandwidth of each user can be further split to multiple sub-bands using digital subcarrier modulation methods for optical-wireless users [57]. The enhanced performance and flexibility offered in this new system architecture opens up new opportunities in software defined networks that enable a simpler and more efficient network resource allocation [58].

As opposed to OPLL used in analog coherent communications and metrology where high bandwidth OPLLs are required to lock the optical phase [49, 59], our approach only requires stabilizing the user transceivers' frequency within a few MHz of the designated comb tone. Thus, it requires only slow and low-cost feedback control. In this proof-of-concept work, the users' CW lasers are tuned to lock to different tones using thermoelectric coolers (TECs). In practice, the user transceivers should automatically lock to the assigned FDM channels. This could be realised using network protocols or physical layer mechanisms.

Conventional wisdom in optical access networks is that tunable lasers and laser control are too costly to implement. Whilst this is true for cost-sensitive optical access systems, the new approach we show

here offers new features to ensure guaranteed bandwidth, low and stable latency, and enhanced power budget (due to low baud rate). The significant progress in laser material and control electronics in the past decade opens up new possibilities to stabilise laser frequency in temperature varying environments [60, 61]. By using the same type of laser for all users, the cost could be brought down significantly with mass production. The frequency comb, user transceivers and coherent receivers can be integrated on readily available InP photonic integration circuit (PIC) platforms [62] and the emerging heterogeneous integration platforms such as III-VI on silicon [63, 64] and thin-film $LiNbO_3$ [65, 66], promising low-cost and low power consumption devices and subsystems.

The impact of the work presented here can be far beyond cloud-user telecommunications. For example, the narrow linewidth laser and the reference clock that seed the comb generator can be synchronised to light sources and clocks in other data centres [59], enabling global carrier frequency and clock synchronization over telecommunication networks for applications such as metrology, passive radar, radio astronomy as well as navigation [67]. The large coverage through telecommunication networks would provide an alternative to the satellite based clock dissemination systems (e.g. GPS) for emergency responses and recovery. Furthermore, clock and frequency synchronised transmission are desired in many applications including quantum links, telescope and micrometer/millimeter wave generation [68] .

4 Methods

4.1 Comb generation and control

We use a RIO ORION laser emitting 13 dBm at 1550.08 nm as the seed source. The CW light is amplified to 33 dBm before being modulated by two PMs and an IM driven with 25-GHz RF signals generated from a low noise RF synthesizer (Rohde & Schwarz SMA100B). The RF signals that drive the PMs are amplified to 33 dBm, yielding a 25-GHz-spacing comb signal with 1.25 THz bandwidth (50 tones). The output of the 1st stage comb generator is split to two branches. The upper branch is filtered and amplified as the LO of the coherent receiver, while the lower branch seeds the 2nd stage comb generator that consists of a PM and an IM. The PM in the 2nd stage is driven with a 2.5 GHz RF signal with 30 dBm power. Both the 25 GHz and the 2.5 GHz RF signals are phase locked to the same 10 MHz reference clock. The generated 2.5-GHz-spacing comb signals has -10 dBm optical power and is subsequently amplified to 18dBm using an EDFA.

4.2 End-user transceivers

We implemented three live user transceivers using the same model of single-wavelength low-cost lasers outputting 8 dBm CW signal with about 150 kHz linewidth [46]. The CW light was split by a 50:50 coupler and mixed with the downstream frequency comb to generate a beat note corresponding to the frequency difference between the CW and the selected reference tone for feedback current control, using a proportional integral (PI) controller. The frequency discriminator is based on analog electronic phase lock loop with 6 MHz locking range.A polarisation controller was used to align the lasers' output to the selected comb tone. This, however, can be eliminated by converting the linear polarisation of the CW to circular polarisation using a quarter wave plate or integrated polarisation converters [69]

The electroabsorption modulators (EAMs) have 10 dB insertion loss and an extinction ratio of more than 10 dB. They are driven with 1.072 GBaud subcarrier (SCM) QAM signals, generated using 4.9 GSa/s digital-to-analog converters (DACs). The digital SCM-QAM signals were generated offline using a pseudorandom binary sequence (PRBS) of 2^{15} length, mapped to QAM symbols, shaped by a root-raise-cosine filter with a 0.01 roll-off factor, and upconverted to a carrier frequency of 0.635 GHz to generate real-value SCM-QAM signals. This allows for a 0.1 GHz gap between DC and the SCM signals in the generated large-carrier double-side band signal (LC-DSB). The frequency and phase noise can be directly estimated from the carrier [70, 71] in the receiver DSP, precluding complex carrier frequency offset (CFO) and carrier phase estimation (CPE) algorithms.

The dummy channels were generated by modulating tapped reference comb signals after transmit through 80 km SSMF for decorrelation. The decorrelated comb passes through a tunable notch filter (30 GHz bandwidth) before combining with the live signals to form the 160 GHz bandwidth upstream signals. The dummy channels are modulated by an MZM driven with 1.072 GBaud intensity-modulated SCM-4QAM signals with a carrier-to-signal-power ratio of about 14 dB, which is similar to that of the live signals. The frequency stability is measured by calculating the spectra of the beat note waveforms.

4.3 Coherent receiver and digital signal processing

The upstream signals are pre-amplified using an EDFA (5 dB noise figure), filtered and detected by a 70 GHz bandwidth dual-polarization coherent receiver. The waveforms were subsequently captured by a 100-GHz-bandwidth 256-GSa/s real-time oscilloscope before performing offline DSP, in which the three user channels were demodulated. The coherent receiver is referenced to the same 10-MHz clock source. Thus, no clock recovery is needed in the DSP. In addition, no dispersion compensation was required due to the low baud rate per user. Since the frequency offset between the user channel and the LO is known, the received live user signals are down converted to base band without needing CFO estimation. The down converted user signals are match filtered and equalized by a pre-trained Volterra filter [72]. BER results for the live user signals are measured using 400000 bits. The sensitivities for SD-FEC threshold are estimated from the BER curves using linear interpolation (supplementary figure S1). The DSP function blocks are detailed in supplementary section IV.

4.4 BER and sensitivity characterization

The sensitivities in shown in figure 4d are calculated from the BER measurement for the live user 1. The BER values are measured by varying the optical power into $EDFA_3$ using a variable optical attenuator (VOA), as shown in figure 3a. The power per user channel was measured using an optical spectrum analyser (OSA) of 0.01nm resolution. The each BER value is calculated using a PRBS of 2^{15} length. The detailed BER results for all live users can be found in the Supplementary section I. The aggregated capacity is calculated by multiplying end user data rate with number of channels achieving sub SD-FEC BER. With 4/8/16QAM, 62, 59 and 56 channels can achieve sub SD-FEC BER. The performance of wavelength channels located at optical bandwidth edge is limited by high frequency roll-off of coherent receiver. With wide-bandwidth coherent receivers, the aggregated data rate could be further improved to 275 Gb/s using SCM-16QAM for all 64 users.

5 Online content

Any methods, additional references, Nature Research reporting summaries, source data, extended data, supplementary information, acknowledgements, peer review information; details of author contributions and competing interests; and statements of data and code availability are available at UCL RPS.

6 Data availability

The data that support the plots within this paper and other findings of this study are available from the corresponding author on reasonable request.

7 Author Contributions

Z.L., Y.L., Z.Z. and K.C prepared the manuscript. Z.L. and J.W. conceived the FDM user multiplexing system architecture. Z.L. and Y.L. conceived the clock and frequency dissemination approach. K.C., R.S and Z.L. developed and implemented the FLL. C.D, R.S., Z.Z. and Z.L. developed the frequency comb source. Z.Z. and C.D. contributed to the phase noise and jitter characterisation. Z.Z. developed the clock synchronisation subsystems and characterise their performance. Z.Z. and Z.L. performed the experiments, including BER and power sensitivity testing, stabilisation of the user lasers, signal generation, coherent detection and associated performance characterisation. E.S. contributed to the coherent signal detection. Z.L., J.W. and Y.L. developed the core digital signal processing. All authors contributed to analysing the experimental results. Z.L. supervised and led the scientific collaboration.

Acknowledgements

The authors acknowledge financial support from EPSRC grants EP/R041792/1, EP/V051377/1, and programme grant TRANSNET EP/R035342/1. The broadband oscilloscope is funded by EPSRC equipment grant EP/V007734/1. The authors also acknowledge the National Natural Science Foundation of China 62102343.

8 Competing Interests Statement

The authors declare no competing interests.

References

[1] Cisco Visual Networking. Cisco annual internet report (2018–2023) white paper. *White paper. Cisco Public, San Jose* (2018).

[2] European Technology Platform Networld 2020. Smart networks in the context of NGI. *Strategic Research and Innovation Agenda 2021-27. Networld Public* (2020). URL `https://www.networldeurope.eu/3487-2/`.

[3] Winzer, P. J. & Neilson, D. T. From scaling disparities to integrated parallelism: A decathlon for a decade. *Journal of Lightwave Technology* **35**, 1099–1115 (2017).

[4] Agrell, E. *et al.* Roadmap of optical communications. *Journal of Optics* **18**, 063002 (2016).

[5] Wang, C. *et al.* Integrated lithium niobate electro-optic modulators operating at CMOS-compatible voltages. *Nature* **562**, 101–104 (2018).

[6] He, M. *et al.* High-performance hybrid silicon and lithium niobate Mach–Zehnder modulators for 100 Gbps and beyond. *Nature Photonics* **13**, 359–364 (2019).

[7] Li, K. *et al.* Electronic–photonic convergence for silicon photonics transmitters beyond 100 Gbps on–off keying. *Optica* **7**, 1514–1516 (2020).

[8] Matsui, Y. *et al.* Low-chirp isolator-free 65-GHz-bandwidth directly modulated lasers. *Nature Photonics* **15**, 59–63 (2021).

[9] Yamaoka, S. *et al.* Directly modulated membrane lasers with 108 GHz bandwidth on a high-thermal-conductivity silicon carbide substrate. *Nature Photonics* **15**, 28–35 (2021).

[10] Koch, U. *et al.* A monolithic bipolar CMOS electronic–plasmonic high-speed transmitter. *Nature Electronics* **3**, 338–345 (2020).

[11] Che, D., Iannone, P., Raybon, G. & Matsui, Y. 200Gb/s bi-directional TDM-PON with 29-dB power budget. In *European Conference on Optical Communication (ECOC)*, We4F–1 (IEEE, 2021).

[12] Zhang, J. *et al.* Demonstration of 100-Gb/s/λ PAM-4 TDM-PON supporting 29-dB power budget with 50-km reach using 10G-class O-band DML transmitters. In *Optical Fiber Communication Conference*, Th4C–3 (Optica, 2019).

[13] Harstead, E., van Veen, D., Houtsma, V. & Dom, P. Technology roadmap for time-division multiplexed passive optical networks (TDM PONs). *Journal of Lightwave Technology* **37**, 657–664 (2018).

[14] Bonk, R. The future of passive optical networks. In *International Conference on Optical Network Design and Modeling (ONDM)*, 1–3 (IEEE, 2021).

[15] Simsek, M., Aijaz, A., Dohler, M., Sachs, J. & Fettweis, G. 5G-enabled tactile internet. *IEEE Journal on Selected Areas in Communications* **34**, 460–473 (2016).

[16] Dohler, M. *et al.* Internet of skills, where robotics meets AI, 5G and the Tactile Internet. In *European Conference on Networks and Communications (EuCNC)*, 1–5 (IEEE, 2017).

[17] Huawei iLab-Ultimate Experience. *Cloud VR Network Solution (white paper)* (Huawei iLab-Ultimate Experience, 2018).

[18] Ericsson and Deutsche Telekom. *Enabling time-critical applications over 5G with rate adaptation (white paper)* (Ericsson and Deutsche Telekom, 2021).

[19] Bonk, R. & Pfeiffer, T. New use cases for PONs beyond residential services. In *Optical Fiber Communication Conference*, Tu2G–1 (Optica, 2022).

[20] Simmons and Simmons. New German draft law on autonomous driving. URL `https://www.simmons-simmons.com/en/publications/cklcdtylu2wtt0970pwjocnti/new-german-draft-law-on-autonomous-driving`. Accessed: 2022-03-23.

[21] Sakaguchi, K. *et al.* Towards mmwave V2X in 5G and beyond to support automated driving. *IEICE Transactions on Communications* (2020).

[22] 3GPP. 5G: Service requirements for enhanced V2X scenarios (TS 22.186 version 15.3.0 Release 15) (2018).

[23] Bogdoll, D. *et al.* Kiglis: smart networks for smart cities. In *IEEE International Smart Cities Conference (ISC2)*, 1–4 (IEEE, 2021).

[24] ResearchAndMarkets.com. Autonomous driving high-precision positioning: 2018-2019 industry report. URL `https://www.businesswire.com/news/home/20190311005756/en/Autonomous-Driving-High-Precision-Positioning-2018-2019-Industry-Report---ResearchAndMarkets.com`. Accessed: 2022-03-23.

[25] Cui, Y. & Ge, S. S. Autonomous vehicle positioning with GPS in urban canyon environments. *IEEE transactions on robotics and automation* **19**, 15–25 (2003).

[26] Mehmood, M., Saleem, S. & Filjar, R. Eyjafjallajökull volcanic ash 2010 effects on GPS positioning performance in the Adriatic sea region. *Atmosphere* **13**, 47 (2021).

[27] Borkowski, R. *et al.* Operator trial of 100 Gbit/s FLCS-PON prototype with probabilistic shaping and soft-input FEC. In *2021 European Conference on Optical Communication (ECOC)*, We4F–3 (IEEE, 2021).

[28] Kizilkaya, B., Zhao, G., Sambo, Y. A., Li, L. & Imran, M. A. 5G-enabled education 4.0: Enabling technologies, challenges, and solutions. *IEEE Access* **9**, 166962–166969 (2021).

[29] Welch, D. *et al.* Point-to-multipoint optical networks using coherent digital subcarriers. *Journal of Lightwave Technology* **39**, 5232–5247 (2021).

[30] IEEE Std 802.3ca-2020. IEEE standard for ethernet amendment 9: Physical layer specifications and management parameters for 25 Gb/s and 50 Gb/s passive optical networks (2020). URL `https://ieeexplore.ieee.org/document/9135000`.

[31] G.989.2. 40-gigabit-capable passive optical networks 2 (NG-PON2): Physical media dependent (PMD) layer specification - amendment 1 (2020). URL `https://www.itu.int/rec/T-REC-G.989.2`.

[32] Bidkar, S., Bonk, R. & Pfeiffer, T. Low-latency TDM-PON for 5G Xhaul. In *International Conference on Transparent Optical Networks (ICTON)*, 1–4 (2020).

[33] eCPRI specification v2.0 (2019). URL `http://www.cpri.info/downloads/eCPRI_v_2.0_2019_05_10c.pdf`.

[34] G.9807.1. 10-gigabit-capable symmetric passive optical network (XGS-PON) (2016). URL `https://www.itu.int/rec/dologin_pub.asp?lang=e&id=T-REC-G.9807.1-201606-I!!PDF-E&type=items`.

[35] Grobe, K. & Elbers, J.-P. PON in adolescence: from TDMA to WDM-PON. *IEEE Communications Magazine* **46**, 26–34 (2008).

[36] Musumeci, F. *et al.* Optimal BBU placement for 5G C-RAN deployment over WDM aggregation networks. *Journal of Lightwave Technology* **34**, 1963–1970 (2016).

[37] Luo, Y. *et al.* Time-and wavelength-division multiplexed passive optical network (TWDM-PON) for next-generation PON stage 2 (NG-PON2). *Journal of lightwave technology* **31**, 587–593 (2012).

[38] Tran, N.-C., Tangdiongga, E., Okonkwo, C., Jung, H.-D. & Koonen, T. Flexibility level adjustment in reconfigurable WDM-TDM optical access networks. *Journal of Lightwave Technology* **30**, 2542–2550 (2012).

[39] Lavery, D. *et al.* A 32x10 Gb/s OLT using a single ultra-wide bandwidth dual local oscillator coherent receiver. In *IEEE Photonics Conference (IPC) Part II*, 1–2 (IEEE, 2017).

[40] Masanet, E., Shehabi, A., Lei, N., Smith, S. & Koomey, J. Recalibrating global data center energy-use estimates. *Science* **367**, 984–986 (2020).

[41] 1588-2019, I. IEEE standard for a precision clock synchronization protocol for networked measurement and control systems (2019). URL `https://standards.ieee.org/ieee/1588/6825/`.

[42] G.8261. Timing and synchronization aspects in packet networks (2008). URL `https://www.itu.int/rec/T-REC-G.8261`.

[43] 802.1CM-2018. IEEE standard for local and metropolitan area networks – time-sensitive networking for fronthaul (2018). URL `https://standards.ieee.org/ieee/802.1CM/6236/`.

[44] Torres-Company, V. & Weiner, A. M. Optical frequency comb technology for ultra-broadband radio-frequency photonics. *Laser & Photonics Reviews* **8**, 368–393 (2014).

[45] Kuo, B. P.-P. *et al.* Wideband parametric frequency comb as coherent optical carrier. *Journal of Lightwave Technology* **31**, 3414–3419 (2013).

[46] O'Carroll, J. *et al.* Wide temperature range 0<T<85 °C narrow linewidth discrete mode laser diodes for coherent communications applications. *Optics Express* **19**, B90–B95 (2011).

[47] Malik, A. *et al.* Low noise, tunable silicon photonic lasers. *Applied Physics Reviews* **8**, 031306 (2021).

[48] Feng, Z. *et al.* Comb-locked telecom-grade tunable laser using a low-cost FPGA-based lockbox. In *Conference on Lasers and Electro-Optics (CLEO)*, STu1J–4 (IEEE, 2021).

[49] Balakier, K., Ponnampalam, L., Fice, M. J., Renaud, C. C. & Seeds, A. J. Integrated semiconductor laser optical phase lock loops. *IEEE Journal of Selected Topics in Quantum Electronics* **24**, 1–12 (2017).

[50] Roberts, K., Beckett, D., Boertjes, D., Berthold, J. & Laperle, C. 100G and beyond with digital coherent signal processing. *IEEE Communications Magazine* **48**, 62–69 (2010).

[51] Rosales, R. *et al.* Achieving high budget classes in the downstream link of 50G-PON. *Journal of Optical Communications and Networking* **13**, D13–D21 (2021).

[52] Miyata, Y. *et al.* UEP-BCH product code based hard-decision FEC for 100 Gb/s optical transport networks. In *Optical Fiber Communication Conference*, JW2A–7 (Optical Society of America, 2012).

[53] Trajkovic, M., Blache, F., Debregeas, H., Williams, K. A. & Leijtens, X. J. Increasing the speed of an InP-based integration platform by introducing high speed electroabsorption modulators. *IEEE Journal of Selected Topics in Quantum Electronics* **25**, 1–8 (2019).

[54] Sohanpal, R. *et al.* Parametric frequency comb generation using silicon core fiber. In *Optical Fiber Communications Conference and Exhibition (OFC)*, M5B–5 (IEEE, 2021).

[55] Clara, M. *High-performance D/A-converters: Application to digital transceivers*, vol. 36 (Springer Science & Business Media, 2012).

[56] Xing, S. *et al.* First demonstration of PS-QAM based flexible coherent PON in burst-mode with 300G peak-rate and record dynamic-range and net-rate product up to 7,104 DBGbps. In *Optical Fiber Communication Conference*, Th4A–4 (Optica, 2022).

[57] Lavery, D. *et al.* Opportunities for optical access network transceivers beyond OOK. *Journal of optical communications and networking* **11**, A186–A195 (2019).

[58] Luo, Y., Gao, L. & Huang, J. MINE GOLD to deliver green cognitive communications. *IEEE Journal on Selected Areas in Communications* **33**, 2749–2760 (2015).

[59] Brodnik, G. M. *et al.* Optically synchronized fibre links using spectrally pure chip-scale lasers. *Nature Photonics* **15**, 588–593 (2021).

[60] Latkowski, S. *et al.* Novel widely tunable monolithically integrated laser source. *IEEE Photonics Journal* **7**, 1–9 (2015).

[61] Blumenthal, D. J. *et al.* Frequency stabilized lasers for coherent fiber interconnects in the datacenter (invited talk). In *2019 IEEE Optical Interconnects Conference (OI)*, 1–2 (IEEE, 2019).

[62] Smit, M., Williams, K. & Van Der Tol, J. Past, present, and future of InP-based photonic integration. *APL Photonics* **4**, 050901 (2019).

[63] Chang, L., Liu, S. & Bowers, J. E. Integrated optical frequency comb technologies. *Nature Photonics* **16**, 95–108 (2022).

[64] Doerr, C. & Chen, L. Silicon photonics in optical coherent systems. *Proceedings of the IEEE* **106**, 2291–2301 (2018).

[65] Yu, M. *et al.* Femtosecond pulse generation via an integrated electro-optic time lens. *arXiv preprint arXiv:2112.09204* (2021).

[66] Xu, M. *et al.* High-performance coherent optical modulators based on thin-film lithium niobate platform. *Nature communications* **11**, 1–7 (2020).

[67] Riehle, F. Optical clock networks. *Nature Photonics* **11**, 25–31 (2017).

[68] Drever, R. *et al.* Laser phase and frequency stabilization using an optical resonator. *Applied Physics B* **31**, 97–105 (1983).

[69] Augustin, L., Hanfoug, R., Van der Tol, J., De Laat, W. & Smit, M. A compact integrated polarization splitter/converter in ingaasp–inp. *IEEE Photonics Technology Letters* **19**, 1286–1288 (2007).

[70] Liu, Z., Kim, J.-Y., Wu, D. S., Richardson, D. J. & Slavik, R. Homodyne OFDM with optical injection locking for carrier recovery. *Journal of Lightwave Technology* **33**, 34–41 (2014).

[71] Jansen, S. L., Morita, I., Schenk, T. C., Takeda, N. & Tanaka, H. Coherent optical 25.8-Gb/s OFDM transmission over 4160-km SSMF. *Journal of Lightwave Technology* **26**, 6–15 (2008).

[72] Wei, J., Stojanovic, N. & Xie, C. Nonlinearity mitigation of intensity modulation and coherent detection systems. *Optics Letters* **43**, 3148–3151 (2018).

[73] TransformaInsights. *Human Machine Interface 101: a primer on new emerging AR and VR techniques that enable human interaction with new emerging technical environments (Technology Insight)* (TransformaInsights, 2021).

[74] PwC and Strategy&. *The 2021 Digital Auto Report (Volum 1)-Assessing Global Mobility Market Dynamics* (PwC and Strategy&, 2021).

Virtual Reality (VR)		Connected Car Fleet
Full View	**Field of View**	
Data Rate **>1.6 Gbps**	Data Rate **>870 Mbps**	Data Rate **>1 Gbps**
Latency **<2 ms**	Latency **<2 ms**	Latency **<3 ms**

Table 1: Future data rate and latency requirement of AR/VR devices and connected car fleet. Here, the estimates for VR targets the highest user experience with 24K resolution and a frame rate of 120 [17]. Note that different VR devices and user experience standard are estimated to co-exist in future deployment. Thus, the user transceivers must be flexible to support different data rate and formats. The estimates for the connected car fleet is obtained by considering 'AI drivers' user cases, where the car fleets exchange information including raw sensor data, vehicles' intention and coordination, enabling cooperative perception for AI drivers [22, 21]. In contrast to conventional applications that predominantly requires high bit rate for data transmission (e.g. video streaming), the above time-critical applications require bounded low latency in conjunction with the ability to scale across a large number of consumer devices.

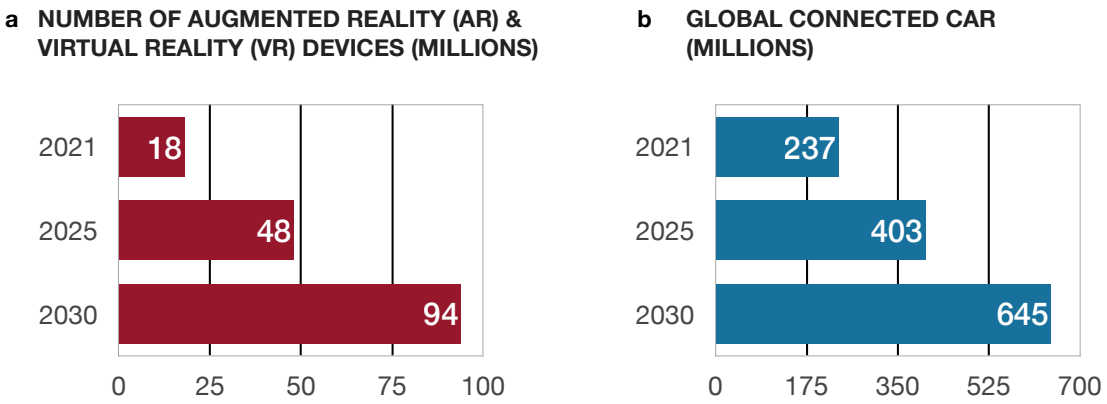

Figure 1: Trends in global increase of (a) VR/AR devices and (b) connected car fleet. a, estimated the number of consumer human machine interface devices dedicated to virtual reality (VR) and augmented reality (AR) in major areas including United States, Europe, China and Japan. The estimation suggests a booming of the AR/VR applications with an average annual growth rate (AAGR) of about 28% from 2021 to 2025, followed by a continuously strong AAGR of about 14% from 2025 to 2030. The VR/AR devices support time-critical applications such as remote surgery, immersive education, teleconference, online gaming and industrial designs [73] b, Estimations summarised collected by PricewaterhouseCoopers (PwC) and Strategy& [74], showing an increase of the connected cars in operation to 403 million by 2025, featuring an average annual growth rate (AAGR) of 14% from 2021 to 2025, followed by an AAGR of 10%, reaching 645 million by 2030. These estimates account for the largest geographical countries for connected cars of the United States, Europe, China and Japan.

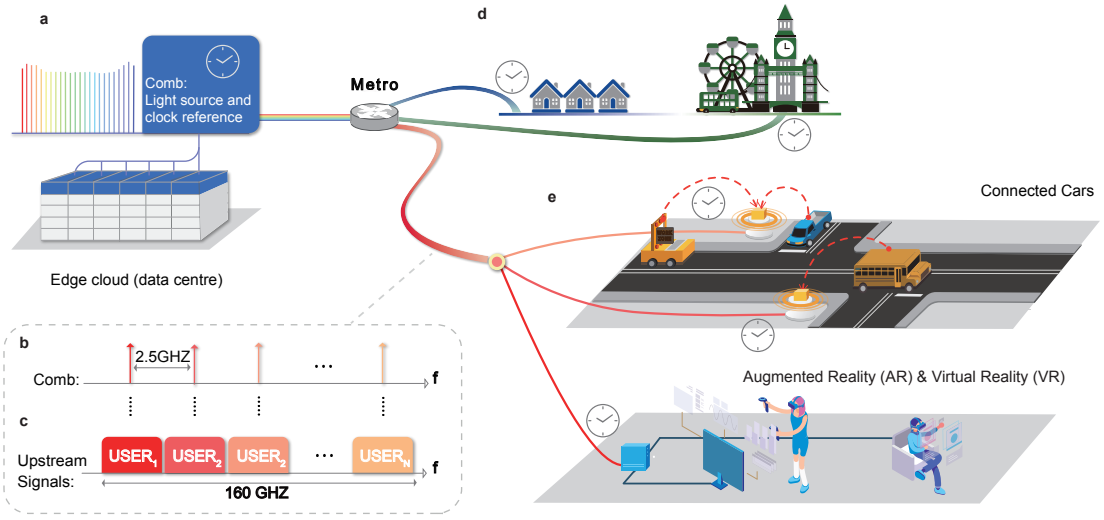

Figure 2: Concept of clock and optical frequency synchornised frequency division multiplexing (FDM) upstream for time-critical applications. a, a wide-bandwidth closely-spaced frequency comb generated at the edge cloud, referenced to a source clock within an edge data centre; b, filtered frequency comb sent from an edge cloud or optical line terminal (OLT) to users; c, upstream FDM signals, each user wavelength locked to a selected tone in the distributed frequency comb, forming a wide bandwidth optical signal which is detected by a single coherent receiver; d, different wavelength division multiplexing band (e.g. 100-200GHz bandwidth) covers different passive split fibre networks. The blue, green and red colour indicate different WDM bands; e, exemplary time-critical applications including cooperative traffic system and virtual reality (VR).

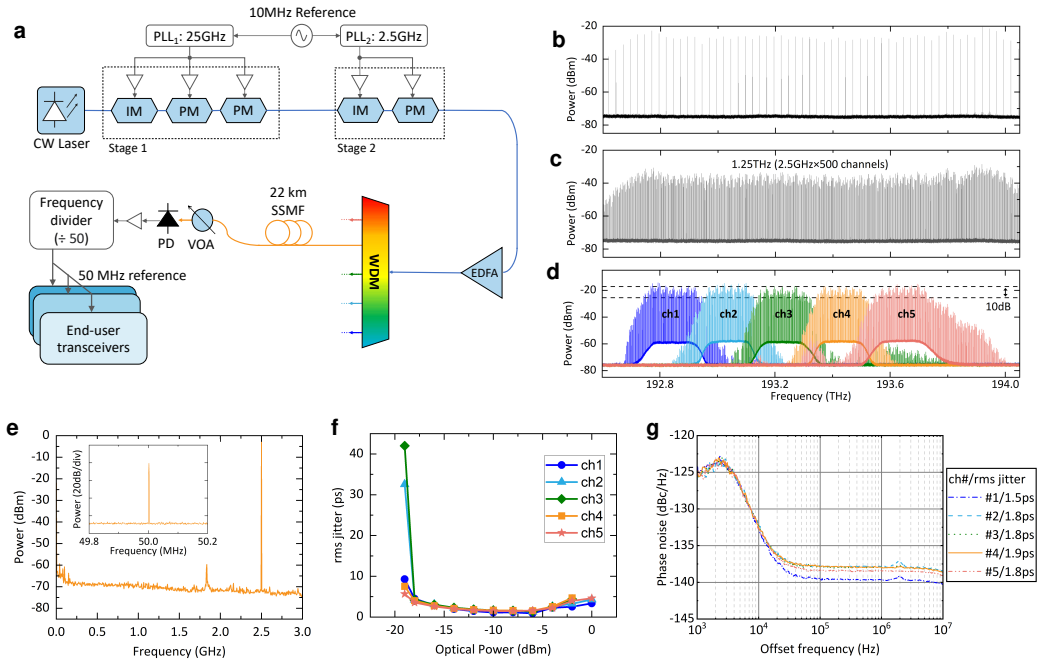

Figure 3: The clock and carrier frequency distribution. a, A continuous wave (CW) laser seeds two stages of comb generator, yielding 1.25-THz bandwidth 2.5-GHz-spacing comb signals with 10-dB flatness. The comb signals are sent to the end-users for clock and carrier frequency synchronisation; b, spectrum of the 25-GHz-spacing comb signals output from the 1st stage, c, spectrum of the generated comb signal output from the 2nd stage; d, demultiplexed comb signals using a 200-GHz WDM each containing 64 2.5-GHz tones with about 10 dB spectral flatness; e, RF spectrum of the detected 2.5-GHz clock signal using channel 4 as example (ITU ch35, 193.4-193.6 THz); f, jitter of the 50-MHz reference clock for end-user transceivers at different received optical power. The increased jitter value from -5 to 0 dBm is due to the saturation of electronic amplifier, the decreased jitter value from -5 to -16 dBm is due to the reduced power; g, measured phase noise of the distributed reference clock signals to different WDM channels, showing a maximum root-mean-square (rms) jitter of <4 ps, integrated over 1 kHz - 10 MHz..

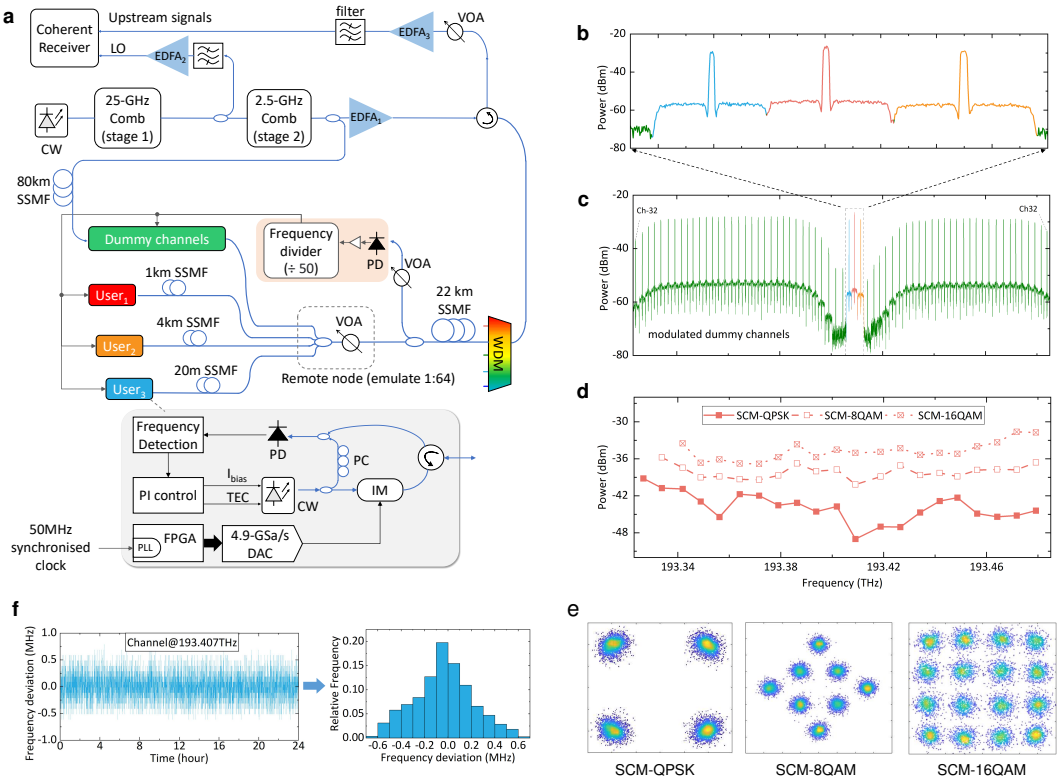

Figure 4: Proof-of-concept experiment for the clock and frequency referenced frequency division multiplexing (FDM) upstream data aggregation for time-critical applications. a, the system diagram of our proof-of-concept experiments with three live end-users combined with dummy signals to form 160 GHz optical bandwidth signals. The optically distributed clock is sent to all live end-user transceivers as the clock reference, based on which three sets of field programmable gate arrays (FPGAs) and 4.9 Gas/s digital to analog converters (DACs) generates SCM-QAM signals and drive the corresponding intensity modulators (IMs) to generate upstream signals. The user lasers generate continuous wave (CW) signals with about 150 kHz linewidth and are frequency-locked to neighbouring comb tones using a frequency lock loop (FLL) containing a frequency detector and a proportional integral (PI) controller, with about 10 kHz loop bandwidth. Thermal-electro controller (TEC) provides feedback for long-term stability and coarse frequency tuning. Two couplers and a 10-dB attenuator are used to emulate 1:64 remote node splitting, resulting in a total link loss of about 28 dB (inc. 22 km SSMF loss, WDM loss, and the remote node splitting loss); b, optical spectrum (20 MHz resolution) of combined upstream signals, with all live transceivers locked to 2.5-GHz-spacing tones; c, optical spectrum (20 MHz resolution) of the upstream signals received: red (user1), orange (user1) and blue (user1). Green indicates the modulated dummy channels; d, measured power sensitivity (power per user signal into EDFA3) for different modulation formats at the soft-decision forward error correction code (SD-FEC) threshold of 2e-2 (15.3% overhead [SD-FEC paper]): cross markers (4QAM), open markers (8QAM), close markers (16QAM); e, measured constellation diagrams of user1; f, measured frequency deviation over 24 hours using user 1 locked at 193.407 THz.

Supplementary Files

This is a list of supplementary files associated with this preprint. Click to download.

- NEsupplementary.pdf